Heliyon 10 (2024) e34221

Contents lists available at ScienceDirect

Heliyon

journal homepage: www.cell.com/heliyon

Research article

T cell proliferation-related subtypes, prognosis model and characterization of tumor microenvironment in head and neck squamous cell carcinoma

Wanjin Jiang [a,b,1], Qi Yang [c,1], Xiaonan Yang [b,1], Ruijia Gan [b], Hongting Hua [b], Zhimin Ding [b], Dongyu Si [b], Xinbei Zhu [f], Xu Wang [e,**], Huabing Zhang [d,***], Chaobing Gao [b,*]

[a] Department of Otorhinolaryngology Head and Neck Surgery, The First Affiliated Hospital of Wannan Medical College Yijishan Hospital, Wuhu, 241000, China
[b] Department of Otorhinolaryngology Head and Neck Surgery, The First Affiliated Hospital of Anhui Medical University, Hefei, 230022, China
[c] Department of Gastroenterology, The First Affiliated Hospital of Wannan Medical College Yijishan Hospital, Wuhu, 241000, China
[d] Department of Biochemistry & Molecular Biology, Metabolic Disease Research Center, School of Basic Medicine, Anhui Medical University, Hefei, 230032, China
[e] Department of General Surgery, The First Affiliated Hospital of Anhui Medical University, Hefei, 230022, China
[f] Department of Otorhinolaryngology Head and Neck Surgery, The Second People's Hospital of Hefei, Hefei, 230011, China

ARTICLE INFO

Keywords:
T cell proliferation-related genes
Prognosis
Tumor microenvironment
Nomogram
Immunotherapy

ABSTRACT

Background: Thirty-three synthetic driver genes of T-cell proliferation have recently been identified through genome-scale screening. However, the tumor microenvironment (TME) cell infiltration, prognosis, and response to immunotherapy mediated by multiple T cell proliferation-related genes (TRGs) in patients with head and neck squamous cell carcinoma (HNSC) remain unclear.

Methods: This study examined the genetic and transcriptional changes in 771 patients with HNSC by analyzing the TRGs from two independent datasets. Two different subtypes were analyzed to investigate their relationship with immune infiltrating cells in the TME and patient prognosis. The study also developed and validated a risk score to predict overall survival (OS). Furthermore, to enhance the clinical utility of the risk score, an accurate nomogram was constructed by combining the characteristics of this study.

Results: The low-risk score observed in this study was associated with high levels of immune checkpoint expression and TME immune activation, indicating a favorable OS outcome. Additionally, various factors related to risk scores were depicted.

** Corresponding author. Department of General Surgery, First Affiliated Hospital of Anhui Medical University, Jixi Road 218, Hefei, 230022, China.

*** Corresponding author. Department of Biochemistry & Molecular Biology, School of Basic Medicine, Anhui Medical University, Meishan Road 81, Hefei, 230032, China.

* Corresponding author. Department of Otorhinolaryngology Head and Neck Surgery, First Affiliated Hospital of Anhui Medical University, Jixi Road 218, Hefei, 230022, China.

E-mail addresses: wx197396@163.com (X. Wang), huabingzhang@ahmu.edu.cn (H. Zhang), gcb110011@163.com (C. Gao).

[1] These authors have contributed equally.

https://doi.org/10.1016/j.heliyon.2024.e34221
Received 31 July 2023; Received in revised form 4 July 2024; Accepted 5 July 2024
Available online 10 July 2024

Conclusion: Through comprehensive analysis of TRGs in HNSC, our study has revealed the characteristics of the TME and prognosis, providing a basis for further investigation into TRGs and the development of more effective immunotherapy and targeted therapy strategies.

1. Background

Head and neck cancer is currently the sixth most common cancer, with approximately 9.32 million diagnoses and approximately 4.44 million deaths per year according to 2020 statistics [1]. Head and neck squamous cell carcinoma (HNSC) is a solid tumor formed by the malignant mucosal epithelium of the pharynx, larynx, and oral cavity accounting for more than 90 % of cases [2]. HNSC is mainly caused by tobacco, alcohol, and human papillomavirus infections [3]. Traditional treatment strategies for HNSC include surgery, radiotherapy, and chemotherapy. HNSC can be cured in its early stage; however, a certain proportion of patients reach an advanced stage, and recurrence or distant metastasis is common. For recurrent/metastatic HNSC (R/M HNSC), conventional therapy has limited efficacy [4]. Indeed, R/M HNSC therapy is a challenging task for clinicians. Tumor immunotherapy is being increasingly considered because of its antitumor effects. Among immune checkpoint inhibitors (ICIs), studies have shown that the survival time of some patients with R/M HNSC can be prolonged by programmed death-1 (PD-1) inhibitors [5]. Biomarker detection, such as PD-1, can assist in the assessment of diagnostic and therapeutic responses to HNSC [6]. However, only a portion of patients with HNSC showed significant results from ICIs treatment. Therefore, the identification of new and promising HNSC biomarkers is necessary to improve the existing HNSC treatment strategies.

The development of malignant tumors is usually accompanied by changes in tumor microenvironment (TME) [7,8]. The TME plays a crucial role in cancer progression and metastasis [9], and encompasses a wide range of cells including immune cells [10]. Among the various cell types in the TME, T cell-related immunotherapy for cancer is receiving increasing attention, with $CD4^+$ and $CD8^+$ T cells emerging as major effectors [11]. Upon recognition of specific antigens via T cell receptors, T cells undergo expansion and initiate the elimination of malignant cells [12]. A recent study identified 33 synthetic driver genes for T cell proliferation through genome-wide large-scale screening [13]. Antitumor effects are characterized by highly coordinated interactions of many genes; however, most current studies have assessed the influence of only one or two T cell proliferation-related genes (TRGs) on HNSC. Therefore, the study of the co-acting characteristics of multiple TRGs may provide clues for the prediction of patient prognosis and discovery of immune characteristics.

Using three computational algorithms, CIBERSORT, ssGSEA and ESTIMATE [14,15], this study aims to comprehensively evaluate the expression profiles of TRGs and to identify data that could be relevant for tumor immunotherapy. Importantly, this study aims provide a basis for predicting tumor prognosis and enhancing our understanding of tumor-related immunology. In addition, qRT-PCR was used to detect the expression of some characteristic TRGs in tumor tissues and adjacent normal tissues of HNSC patients and in 2 HNSC cell lines to identify differences in the expression of these genes.

2. Materials and methods

2.1. Raw data

The obtained TCGA (portal.gdc.cancer.gov) and GEO (ncbi.nlm.nih.gov/geo/) (GSE65858) cohorts were carefully sorted and summarized in detail. A total of 771 patients with HNSC were included in this study (incomplete survival information were excluded) (Table S1).

2.2. Consensus clustering analysis of TRGs

We obtained 33 TRGs from the study results of Legut et al. [13], as shown in Table S2. "ConsensusClusterPlus" and "ggplot2" R package were used for Cluster analysis and Principal component analysis (PCA) respectively, according to different TRGs expression levels. Gene set variation analysis (GSVA) was used specifically for differences in the biological processes and pathways of the TRGs.

2.3. Analysis of the clinical and biological features of the two TRGs subtypes

To observe the prognostic condition of the two TRGs subtypes, a survival analysis was done using survival and survminer R packages. Kaplan-Meier (KM) curves were obtained to evaluate differences in survival time between the two subtypes. TNM stage, age and TRGs expression information were visualized by a heatmap generated by using the pheatmap R package.

2.4. Differences in TME and immune checkpoint expression levels among TRGs subtypes in HNSC

“CIBERSORT” and “ESTIMATE” were performed to measure the abundances of multiple immune cell subsets and different immune scores in different TRGs subtypes in HNSC samples, respectively. The gene expression of single samples in HNSC converted into gene set enrichment profiles using ssGSEA. Differences in immune checkpoint levels among the TRGs subtypes in HNSC were investigated.

2.5. Analysis of differentially expressed genes (DEGs)

DEGs were found among TRG subtypes, and the conditions were set the standard for a false discovery rate (FDR) < 0.05 and $|\text{logFC}| > 0.585$. DEGs were explored using Gene Oncology (GO) and the Kyoto Encyclopedia of Genes and Genomes (KEGG). Using these data we were able to classify the DEGs into three gene subtypes.

2.6. Establishment of prognostic risk score

The initial step involved conducting a univariate Cox analysis of DEGs to identify those that were associated with survival. LASSO (Least absolute shrinkage and selection operator) analysis was performed to reduce the risk of overfitting. HNSC samples were randomly divided into a training set (n = 386) and a testing set (n = 385) in equal proportions. Finally, multivariate Cox analysis was used to screen candidate genes and risk scores were constructed in the training set. The risk score formula is as follows: risk score = $\sum_{i=1}^{n} \beta i * \lambda i$, where n, βi, and λi represent candidate gene numbers, coefficients, and expressions, respectively. The median risk score differentiates between the high- and low-risk groups. Then, according to the set conditions, 386 patients in the training set were divided for K–M analysis and comparison. According to this grouping method, the training, testing, and all sets (all samples in the set) were classified and analyzed for survival. Finally, the receiver operating characteristic (ROC) curves of the training, testing, and all sets were drawn.

2.7. Establishment of a nomogram

Clinical characteristics and risk scores were used to evaluate the results of nomogram using independent prognostic analyses based on the "rms" package. In the nomogram scoring system, each variable corresponds to a score, and the total score of each sample is obtained by adding all the variable scores. Validation curves were used to describe the reliability of 1 -, 3 -, and 5-year survival event predictions.

2.8. Immune status of TME

Initially, we use the “CIBERSORT” algorithm to determine the abundance of immune cells, followed by generating scatter plots of immune cells, risk assessment, as well as heat maps of immune cells and 23 prognostic genes were drawn. Lastly, we calculated the differences between the immune checkpoints and risk scores.

2.9. Cancer stem cell (CSC), mutation and drug sensitivity

CSC refers to cancer cells that have the properties of stem cells, that is, the ability to "self-replicate" and "have multicellular differentiation." Usually such cells are considered to have the potential to form tumors and develop into cancers, especially as the cancer metastasizes out, creating a source of new cancers. Initially, scatter plots of the risk score and CSC index were generated. Subsequently, mutation annotation data were obtained from "maftools," and waterfall plots of somatic mutations in HNSC samples from different risk groups were generated. In addition, the sensitivity to some chemotherapeutic drugs was assessed using "pRRophetic."

2.10. Patient and specimen

Tumor tissues and pairs of adjacent normal tissues (>1 cm from the tumor margin) were collected from 8 patients who underwent surgical resection at the First Affiliated Hospital of Anhui Medical University (Hefei, China) between December 2022 and June 2023. Patients provided signed informed consent prior to the study. Each surgically excised specimen was placed in a refrigerator at −80 °C to extract genomic RNA and proteins. The ethical approval was approved by the Ethics Committee of the First Affiliated Hospital of Anhui Medical University.

2.11. Cell Culture and verified by qRT-PCR and Western blotting

The HNSC cell lines, TU177 and FaDu, were purchased from American Type Culture Collection. Cells were incubated at 37 °C with 5 % CO_2 in DMEM (Gibco) supplemented with 10 % FBS (Lonsera, Australia), penicillin (100 U/ml) and streptomycin (100 mg/ml, Biosharp, China). All cells were grown at 37 °C in a humidified atmosphere with 5 % CO_2.

Gene expression was detected by qRT-PCR. RNA was isolated from HNSC tissues and cell lines by TRIzol kit (Carlsbad, CA, USA), and its concentration was determined by ultraviolet spectrophotometry. The PrimerScript RT Master then reverse-transcribed the RNA into cDNA. The concentration of cDNA was determined by SYBR Green PCR master mixture and LightCycler 96 system (Roche). The relative expression levels of ULBP2, NKX2-3, CLEC3B, CSF2 and FGD3 mRNA were quantified by $2-\Delta\Delta Cq$ normalized to 36B4. Gene-specific primers are listed in Table S8.

For Western blot analysis, total proteins were extracted from cells using RIPA buffer (Beyotime, China). The same amount of protein was separated by sodium dodecyl sulphate-polyacrylamide gel and transferred to a polyvinylidene fluoride (PVDF) membrane, which was sealed with 5 % skim milk at room temperature for 1 h and incubated overnight at 4 °C with primary antibody ULBP2(ab275023,

abcam, 1:1000) and β-actin (#4970, Cell Signaling Technology, 1:1000). Then HRP conjugated secondary antibody was incubated at room temperature for 1 h. Protein bands were quantitatively analyzed by ECL on chemiluminescence apparatus.

2.12. Construction of small interfering RNA (siRNA) and transfection of HNSC cell lines

The siRNAs targeting ULBP2 were constructed (GenePharma Co., Ltd., Shanghai). The sequences were as follows: si-NC (5'-UUCUCCGAACGUGUCACGUTT -3') and si-ULBP2(5′-CAACAAGACAGUCACACCUTT-3′). Cells were grown to 50 % confluence and were transfected using Lipofectamine 3000 (Invitrogen, Shanghai, China) based on the protocol of the manufacturer. To verify the efficiency of ULBP2 downregulation by siRNA, tumour cells were seeded in 6-well plates. After incubating for 48 h, cells were washed and used for subsequent experiments.

2.13. Cell viability assay and clone formation assay

Two cell lines mentioned above were used for *in vitro* studies. For the cell viability assay, cells were pretreated with si-NC or si-ULBP2 and a total of 2000 cells were seeded in each 96-well plates. After culture for 0, 24, 48, or 72 h, 25 μl MTT solution (Solarbio, Shanghai, China) was added to each well, and returned to the incubator for a 1 h incubation. Then the medium was discarded, 100 μl DMSO was added to each well and incubated for 10 min. Finally, the absorbance value of each well at OD490 nm was measured using a microplate analyzer.

For the clone formation assay, cells were pretreated with si-NC or si-ULBP2, and 2000 cells were seeded in each 6-well plates. After 1 week of culture, the total number of clones was calculated after fixation with 4 % paraformaldehyde for 15min and staining with crystal violet at room temperature for 10min.

2.14. Statistical analyses

All scripts were run in Strawberry-Perl-5.30.0 and all codes were run in R 4.2.1. *In vitro* analyses were performed in triplicate. Data

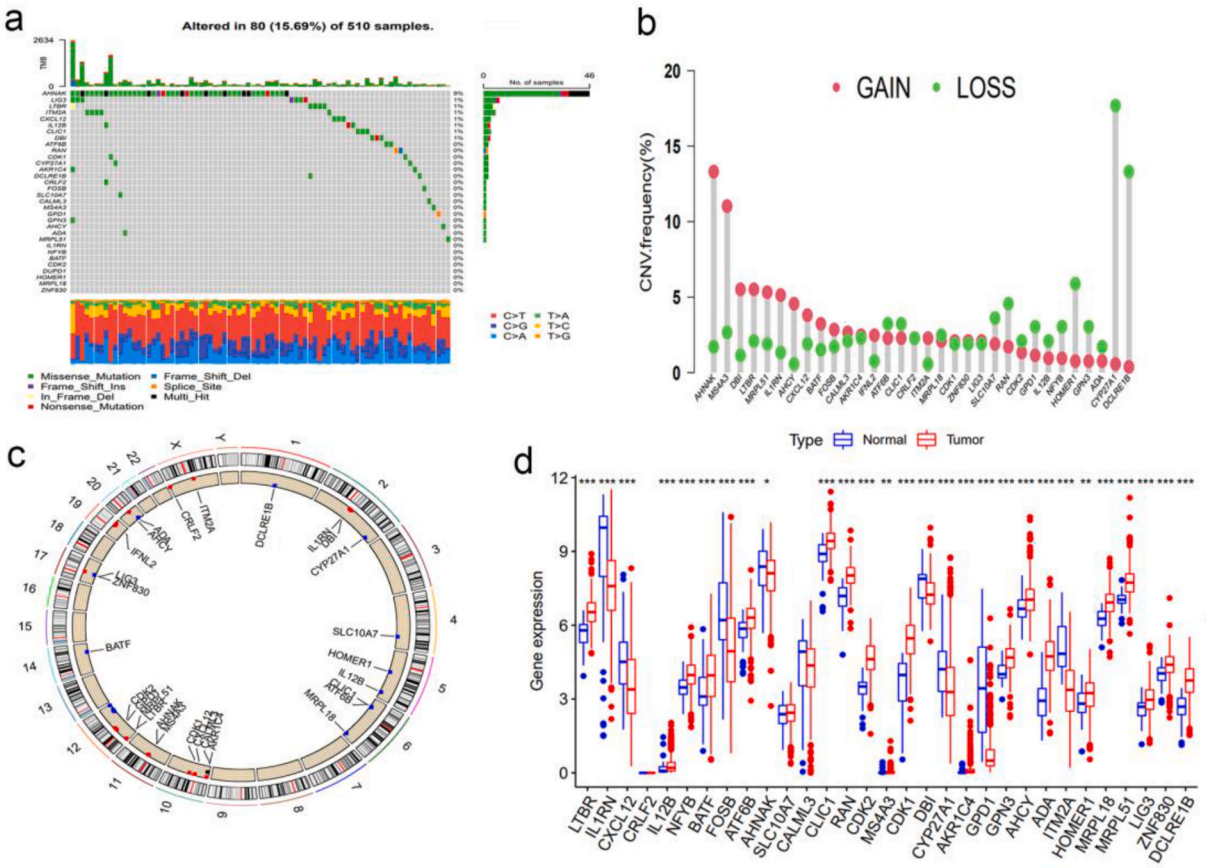

Fig. 1. Mutation, CNV, and expression of TRGs in HNSC (a) Mutation of 33 TRGs in 510 patients with HNSC. (b) CNV variation of TRGs. (c) The CNV alterations of TRGs position on 23 chromosomes. (d) Expression of 33 TRGs in normal and HNSC tissues.

are means ± SD and were compared with GraphPad Prism 9.0 using Student's t-tests or one-way ANOVAs. Statistical significance was defined as $P < 0.05$. *$P < 0.05$, **$P < 0.01$, ***$P < 0.001$.

3. Results

3.1. Mutation and copy number variation (CNV) of TRGs in HNSC

Somatic mutations were found in 33 TRGs in 80 (15.69 %) of the 510 samples. The mutation frequencies from high to low were AHNAK, LIG3, LTBR, ITM2A, CXCL12, IL12B, CLIC1, and DBI, while the other TRGs did not have any mutations (Fig. 1a). Moreover, 33 TRGs of somatic CNV were found to be common. CNV increased in AHNAK, MS4A3, DBI, LTBR, MRPL51, IL1RN, and AHCY and decreased in AHNAK, MS4A3, DBI, LTBR, MRPL51, IL1RN, and AHCY (Fig. 1b). The position of the CNV on chromosomes in TRGs is shown in Fig. 1c. Factors that regulate gene expression include CNV, DNA methylation, transcription factors, among others [16,17]. The analysis results showed that mRNA expression of HNSC and normal tissue samples was significantly different (Fig. 1d), indicating a potential role of TRGs in HNSC genesis.

3.2. TRGs subtypes were obtained by consensus clustering

The research process is illustrated in Fig. S1. The characteristics of the included patients with HNSC were shown in Table S1. First, K–M and univariate Cox regression analyses were performed to determine the effects of the 33 TRGs on the prognosis of patients with HNSC (Fig. S2 and Tables S2 and 3), and TRGs regulatory connections and interactions were demonstrated through the TRGs network (Fig. 2a). The consensus clustering algorithm was used in this study to obtain TRGs subtypes to analyze the expression characteristics of prognostic TRGs in HNSC (Fig. S3). $k = 2$ was the best choice, that is, subtypes A ($n = 507$) and B ($n = 264$) (Fig. 2b). The expression of the two TRG subtypes was distinct different, as shown by the PCA analysis (Fig. 2c). Crucially, the K–M curve showed that patients with subtype B had better survival (log-rank test, $p = 0.005$; Fig. 2d). Finally, the heat map showed differences in TRGs expression levels among the different subtypes (Fig. 2e).

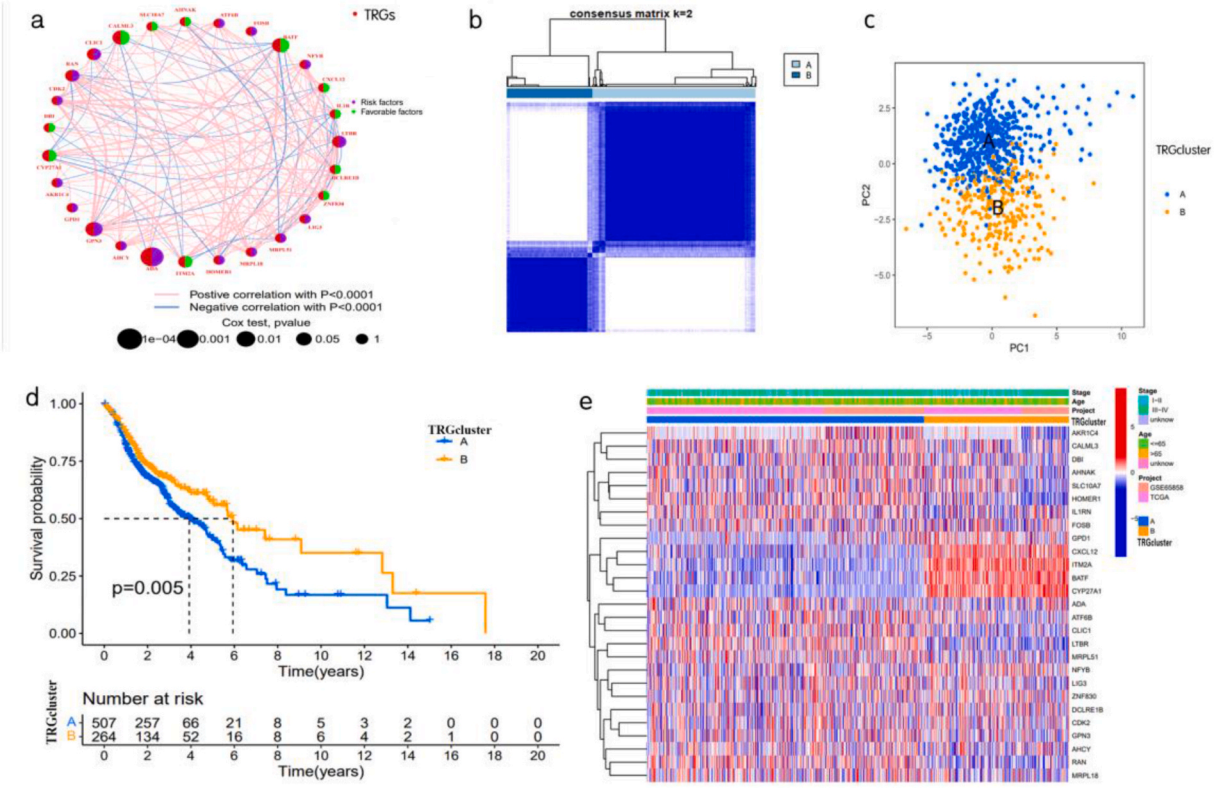

Fig. 2. Identification of two distinct TRG subtypes in 771 samples. (a) TRGs interaction in HNSC. The thickness of the lines connecting TRGs indicates the strength of the association between TRGs. Pink means positive correlation, blue means negative correlation. (b) The consensus matrix heatmap defined two TRG clusters. (c) PCA analysis between the two TRG subtypes. (d) Kaplan-Meier curve showed a significant difference in survival time between the two TRG subtypes (log-rank test, $p = 0.005$). (e) Differences in expression levels of TRGs between two different TRG subtypes.

3.3. TME differences in TRGs subtypes

First, according to the GSVA results, subtype B was abundant in the immune activation (Fig. 3a–b; Table S4). The abundance of multiple immunoinfiltrating cells (Table S5), showed that the infiltration of most immune cells of subtype B was significantly higher (Fig. 3c). Similarly, immune checkpoint analysis showed significantly elevated expression of subtype B at all eight immune checkpoints (Fig. 3d). Finally, the immune scores were evaluated, and the analysis showed that patients with subtype B with better prognosis still had higher immune scores in the TME (Fig. 3e).

3.4. Screening of DEGs and search for gene subtypes

Through "limma" package, 1270 DEGs were identified based on TRG subtypes, set the standard for FDR <0.05 and $|\log FC| > 0.585$. Using GO and KEGG, biological functions and pathways of DEGs were identified (Fig. 4a–b; Table S6), these 1270 genes were mainly related to immune-related biological function and pathways. Finally, to analyze the prognostic value of 1270 DEGs, 307 DEGs related to survival were screened, and the samples were divided into three genomic subtypes: A, B, and C (Fig. 4c). The heat map and boxplot showed significant differences in the expression of DEGs and TRGs in the three gene subtypes (Fig. 4d–e). These results demonstrated that TRGs play a fundamental role in immune-related processes and prognosis.

3.5. Establishment of a prognostic risk score

Fig. 5a shows the allocation of patients with HNSC into two TRG subtypes, three genetic subtypes, and two risk groups. For example, it can be seen that TRG subtype B is more closely associated with genetic subtype C, and genomic subtype C is more closely associated with low-risk group, and the probability of good prognosis is greater in low-risk groups. First, to reduce collinearity and overfitting of the model, we used LASSO regression analysis to analyze 307 prognostic related DEGs. As shown in the LASSO regression analysis and partial likelihood deviance curves, 44 survival related genes were obtained (Fig. 5b–c). Then, 23 genes were finally obtained by multivariate Cox regression analysis (Table S7), including 11 high-risk genes (CCL19, ATP2A3, SH3KBP1, ARL4D, CPVL, LPL, ULBP2, HOXC13, SFRP2, IGFL1, and CSF2), and 12 low-risk genes (CTLA4, ANKRD44, FGD3, CLEC3B, LIMD2, and CTSG, NKX23, DSC3, PTPRZ1, ODAM, SPINK6, and TFF3). Moreover, the risk score for subtype C was the lowest among the three gene subtypes (Fig. 5d). Of the two TRG subtypes, subtype B with a higher immune score had a lower risk score; therefore, a lower risk score might be associated with immune activation (Fig. 5e). In particular, the expression levels of most TRGs differed significantly between the two risk groups (Fig. 5f) and the gene expression results were similar to those previously reported.

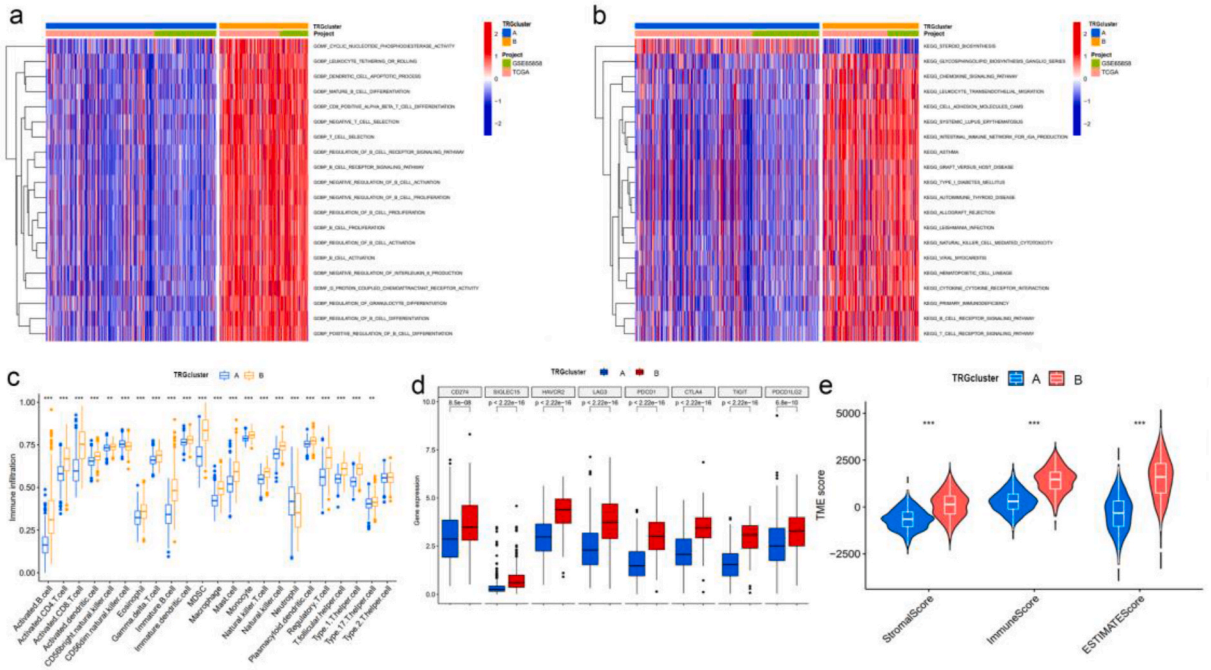

Fig. 3. Differences in TME between two TRG subtypes (a–b) GSVA of biological Process and pathways between two TRG subtypes. (c) Abundance of multiple infiltrating immune cell types in two TRG subtypes. (d) Expression levels of immune checkpoints between two TRG subtypes. (e) Differences in TME score between two TRG subtypes.

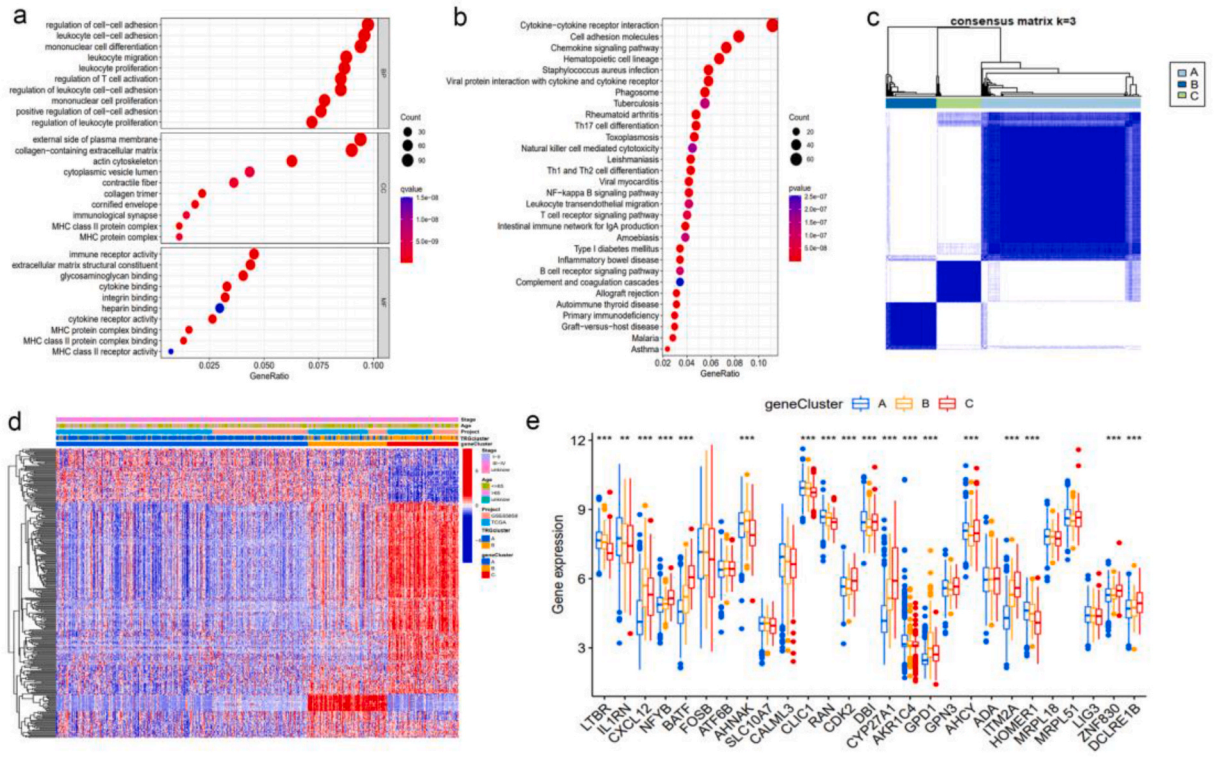

Fig. 4. Identification of three distinct genetic subtypes based on DEGs between two TRG subtypes (a) GO analysis of DEGs. (b) KEGG analysis of DEGs. (c) Three gene clusters were identified by consensus matrix heat maps. (d) Differences in DEGs expression levels of different gene subtypes. (e) Differences in TRGs expression levels among different gene subtypes.

3.6. Evaluation of prognostic models

Risk ranking points and scatter plots showed that patients with high-risk scores were more likely to die, and heat maps were used to show the differential expression of 23 prognostic-related genes (Fig. 6a–c). KM showed that the prognosis in the low-risk group was significantly better (log-rank test, $p < 0.001$; Fig. 6d–f). Analysis of 1-year, 3-year, and 5-year prognostic efficiency showed that the risk score had a high AUC value, suggesting that the risk score had good predictive power for survival in HNSC (Fig. 6 g-i). These results were consistent across the training, testing, and across all sets.

3.7. Establishment of a nomogram

Forest maps illustrated that age, clinical stage, and risk score were important prognostic factors for patients with HNSC (Fig. 7a and b). These factors were used to construct nomogram models for HNSC (Fig. 7c). For example, the 1-year, 3-year, and 5-year survival rates of a 65-year-old patient with stage III-IV disease were 71.7 %, 36.8 %, and 22.8 %, respectively. Finally, calibration plots showed that the nomogram had good prediction ability (Fig. 7d).

3.8. TME and immune checkpoint with risk score

First, scatter plots showed that immune cells were significantly correlated with risk scores, with an overall trend. At that time, the correlation coefficient was low, which was worthy of further discussion (Fig. 8a). The heat map showed that most immune cells were significantly associated with the 23 prognostic genes (Fig. 8b). Finally, the boxplot showed that the expression of most immune checkpoints was significantly correlated with risk scores (Fig. 8c).

3.9. CSC, mutation and drug sensitivity

Fig. 9a shows that HNSC cells with lower risk scores were characterized by more stem cells. The results of Fig. 9b–c indicated that 226 (97 %) of 233 high-risk groups had gene mutations and 238 (90.84 %) of 262 low-risk groups had gene mutations, among which TP53 and TTN had the highest mutation frequency. However, the boxplot and scatter plot (Fig. 9d–e) showed no significant difference between the risk score and TMB, suggesting that the potential role of mutations between different risk groups may not be significant.

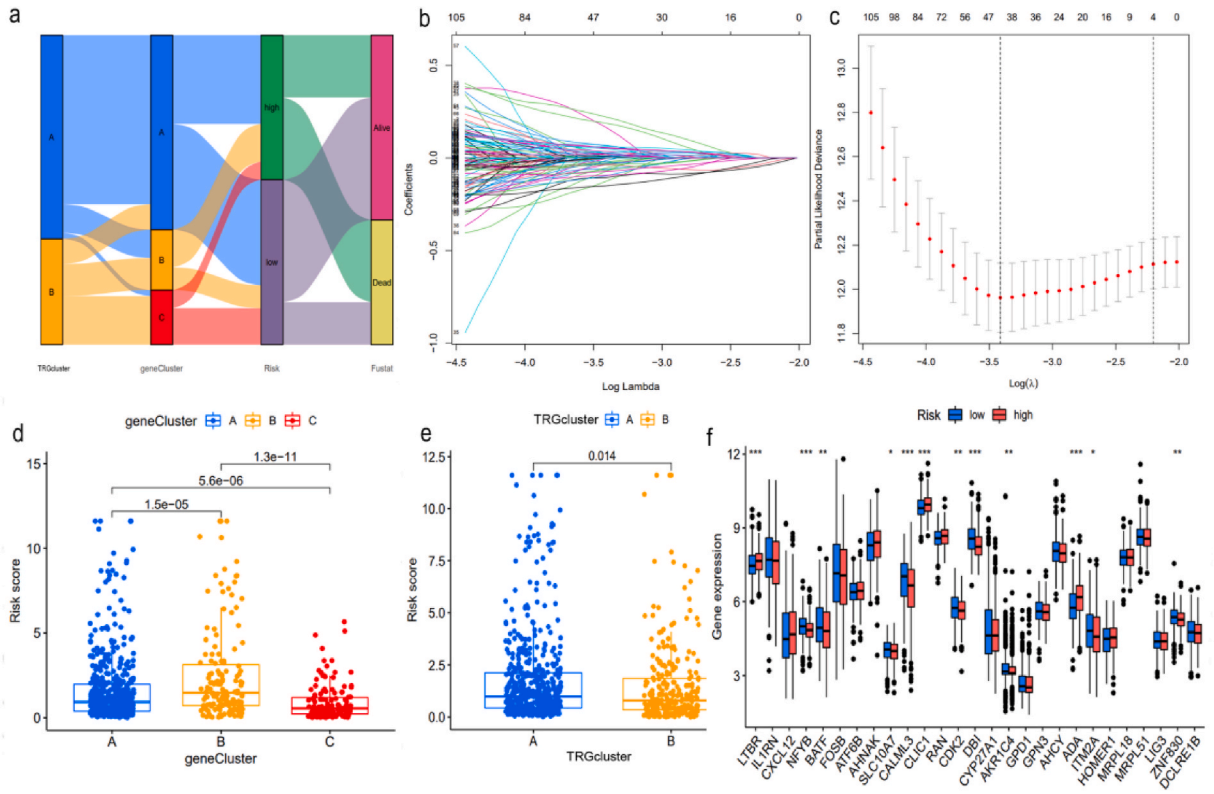

Fig. 5. Establishment of a prognostic risk score. (a) Alluvial diagram of TRG subtypes, gene subtypes, risk score and prognosis. (b–c) The LASSO analysis and partial likelihood deviance of prognostic DEGs. (d) Relationship between three gene subtypes and risk scores. (d) Relationship between two TRG subtypes and risk scores. (f) Expression levels of TRGs between high-risk and low-risk score groups.

Finally, we found that the low-risk group had a significantly lower IC50 for chemotherapy drugs such as methotrexate, mitomycin, and vinorelbine, suggesting that the risk score may also be potentially related to drug sensitivity (Fig. 9f–i).

3.10. Comparison of the expression levels of the partial prognostic signature TRGs between tumor and normal control samples

Five of the 23 prognostic related genes were selected by random number method, and the boxplot was used to describe the different expression levels of five characteristic TRGs between HNSC patients and normal control samples in the TCGA database (Fig. 10a). We further collected cancer tissues and adjacent tissues of 8 HNSC patients from the First Affiliated Hospital of Anhui Medical University. qRT-PCR was used to detect the relative mRNA expression levels of 5 characteristic TRGs in cancer tissues and adjacent tissues. In Fig. 10c, we found that the expression levels of four characteristic genes (ULBP2, CLEC3B, CSF2, and FGD3) in tumor tissue cells were significantly different from those in corresponding normal tissues, confirming our previous results.

3.11. Knocking down ULBP2 inhibits cell proliferation

The KM curve showed that patients with low ULBP2 expression had longer OS (Fig. 10b). We further compared the differences in ULBP2 protein expression between cancer tissues and adjacent tissues of 8 HNSC patients, and found that ULBP2 protein expression was significantly increased in cancer tissues (Fig. 10d). To explore the biological function of ULBP2 in HNSC, we added si-ULBP2 to TU177 and FaDu cell lines, and qPCR and Western blot results showed that the mRNA and protein expression levels of ULBP2 in the knocked down cell lines were significantly reduced compared to control cells (Fig. 10e–f). To determine the effect of ULBP2 on the proliferation ability of HNSC cells, we performed the MTT assay and the colony formation assay. MTT experiments showed that knocking down ULBP2 could inhibit cell viability (Fig. 10g), and the colony formation experiment showed that knocking down ULBP2 could also decrease colony-forming abilities (Fig. 10h).

4. Discussion

Through genome-wide large-scale screening, a recent study identified 33 T cell-proliferating genes associated with immunity and antitumor activity [13,18]. However, the potential usefulness of these TRGs in the TME, prediction of prognosis in patients with HNSC,

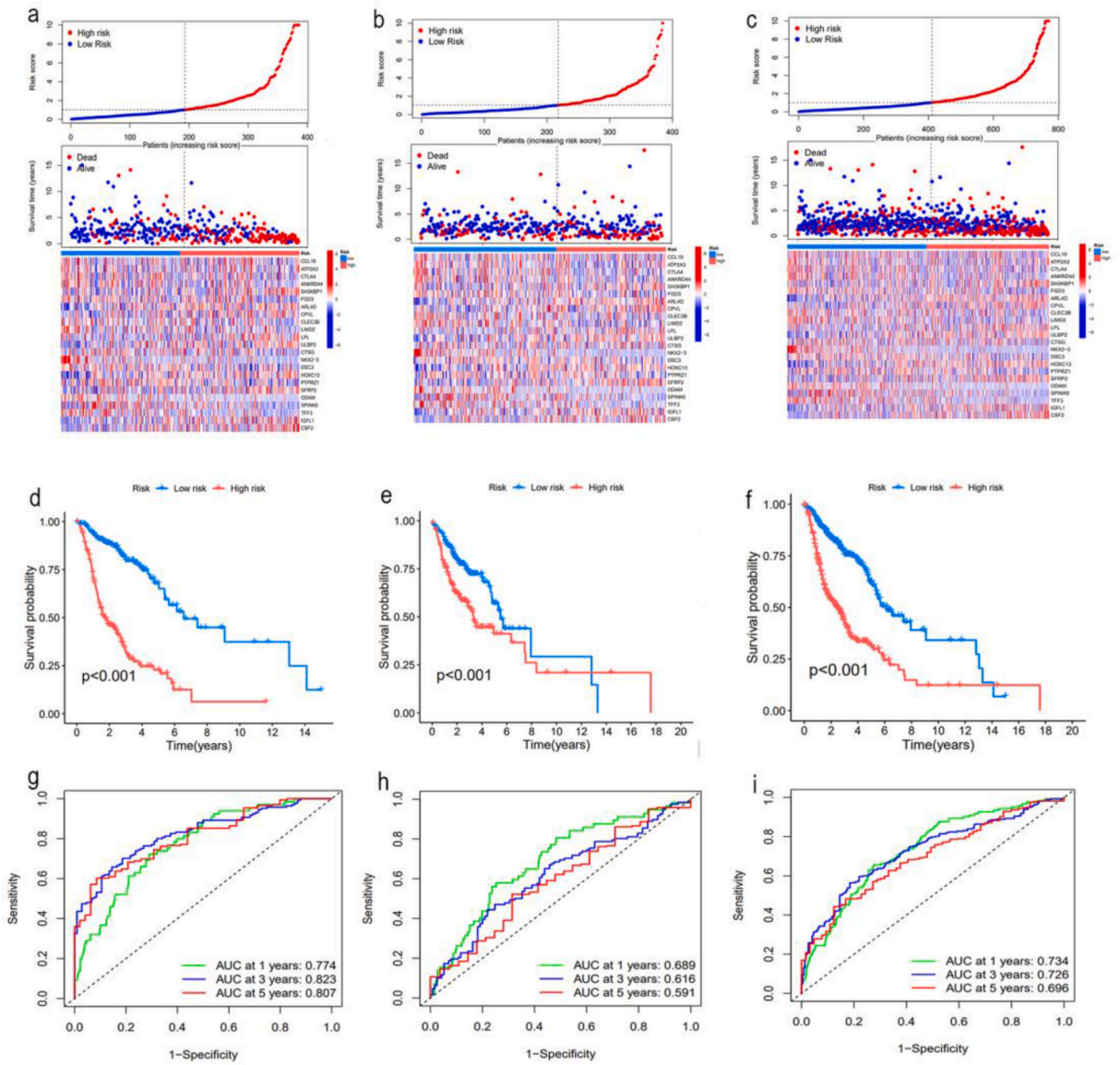

Fig. 6. Comprehensive utility and evaluation of risk scores. (a–c) Ranked dot and scatter plots showed risk scores and prognosis, and heatmaps showed the expression of prognostic risk genes between training, testing, and all set. (d–f) Kaplan Meier analysis showed that OS rate of high-risk patients was significantly lower than that of low-risk patients between training, testing, and all set. (g–i) ROC curves were used to evaluate 1-, 3-, and 5-year survival between training, testing, and all set.

and exploration of immunotherapeutic biomarkers have not been fully studied. Some of these individual TRGs have been shown to be associated with multifarious tumors; for example, activation of the LTBR signaling pathway can involve different types of cancer cells [19]. The invasion of urothelial carcinoma with excessive expression of IL1RN is significantly reduced [20], and CXCL12 supports signaling pathways associated with lymph node metastasis [21]. BATF served as a key anti-tumor target in regulating the function of $CD8^+$ T cells and mitochondria [22], and elevated AHNAK content could repress ovarian cancer cell growth [23]. However, most previous studies focused on one or two TRGs or TME cells. Therefore, we fully characterized the global effects and TME penetration mediated by the multiple TRGs combinations. Our study revealed the transcriptional alterations, genetic levels, and prognostic value of TRGs in HNSC. Transcripts, along with their genes, help elucidate the mechanisms of carcinogenesis [24] and improve biomarker discovery and therapeutic benefits [25]. We obtained two different molecular subtypes based on 33 TRGs. This study found that subtype B had significantly better OS, and TRGs expression differed significantly among the different TRG subtypes in patients with HNSC. This suggests that the transcriptional alterations and genetic levels of TRGs affect the prognosis of HNSC.

The genes constructing prognostic characteristics were screened through LASSO and multivariate Cox analysis, and 23 characteristic genes were screened for the calculation of the risk score. Among these 23 signature genes, some have been shown to be

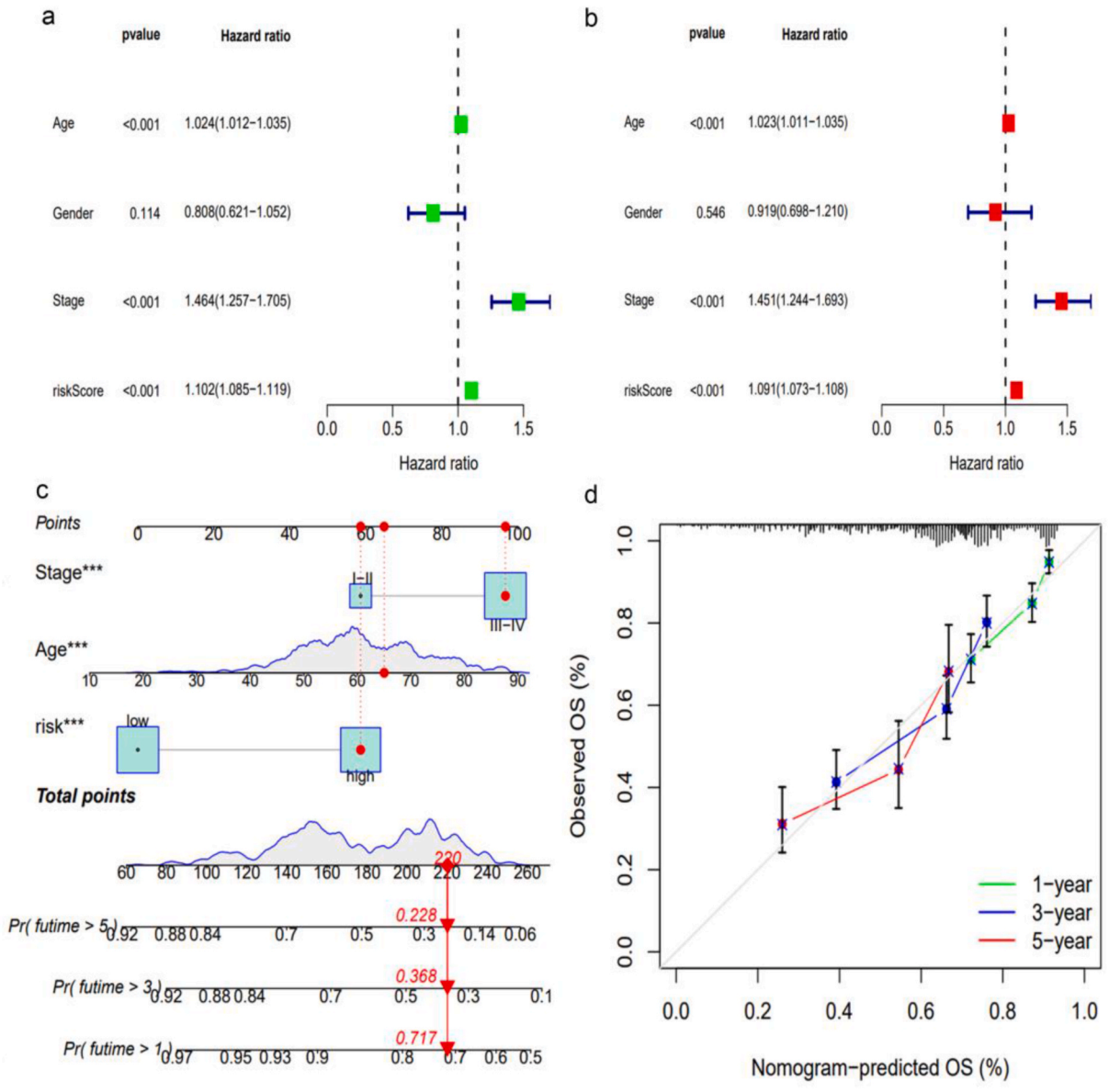

Fig. 7. Establishment and validation of a nomogram. (a–b) Univariate and multivariate regression analysis of HNSC patients. (c) Nomogram for predicting the 1-, 3-, and 5-year OS of HNSC patients. (d) Calibration curves indicate the accuracy and specificity of the nomogram for predicting of 1-, 3-, and 5-year OS.

associated with HNSC or other tumors. For example, CCL19 is one of the 12 potential prognostic markers of overall survival in HNSC [26]. ATP2A3 may guide clinical immunotherapy for HNSC [27]. CTLA4 was identified as a marker gene enriched in oral squamous cell carcinoma and potentially linked to tumor immunosuppression [28]. Survival analyses have shown that FGD3 is associated with survival in patients with HNSC [29]. Inactivated SFRP2 impairs cancer cell migration [30]. CSF2 activates anti-apoptotic and pro-angiogenic pathways in tumor cells [31]. CSF2 and CTLA4 are potential biomarkers and therapeutic targets for HNSC [32]. In this study, 23 integrated signature genes were used to predict patient prognosis and provide information for individualized immune-related therapies. Risk score, clinical stage, and age are found to be important prognostic factors. As nomograms have been widely used as a predictive tool for cancer [33,34], to better understand the clinical characteristics and role of risk scores, we developed nomogram models and validated their high predictive efficiency. As mentioned above, our risk score strongly influenced the prognosis of patients with HNSC.

The treatment of HNSC remains challenging [35]; immunotherapy has achieved good results in a proportion of patients with R/M HNSC in recent years, but the prognosis of patients with HNSC is still inconsistent, which highlights that the TME is crucial in HNSC [36–38]. The main immune cells in the TME are T cells, B cells, and macrophages, which are the key effectors involved in the

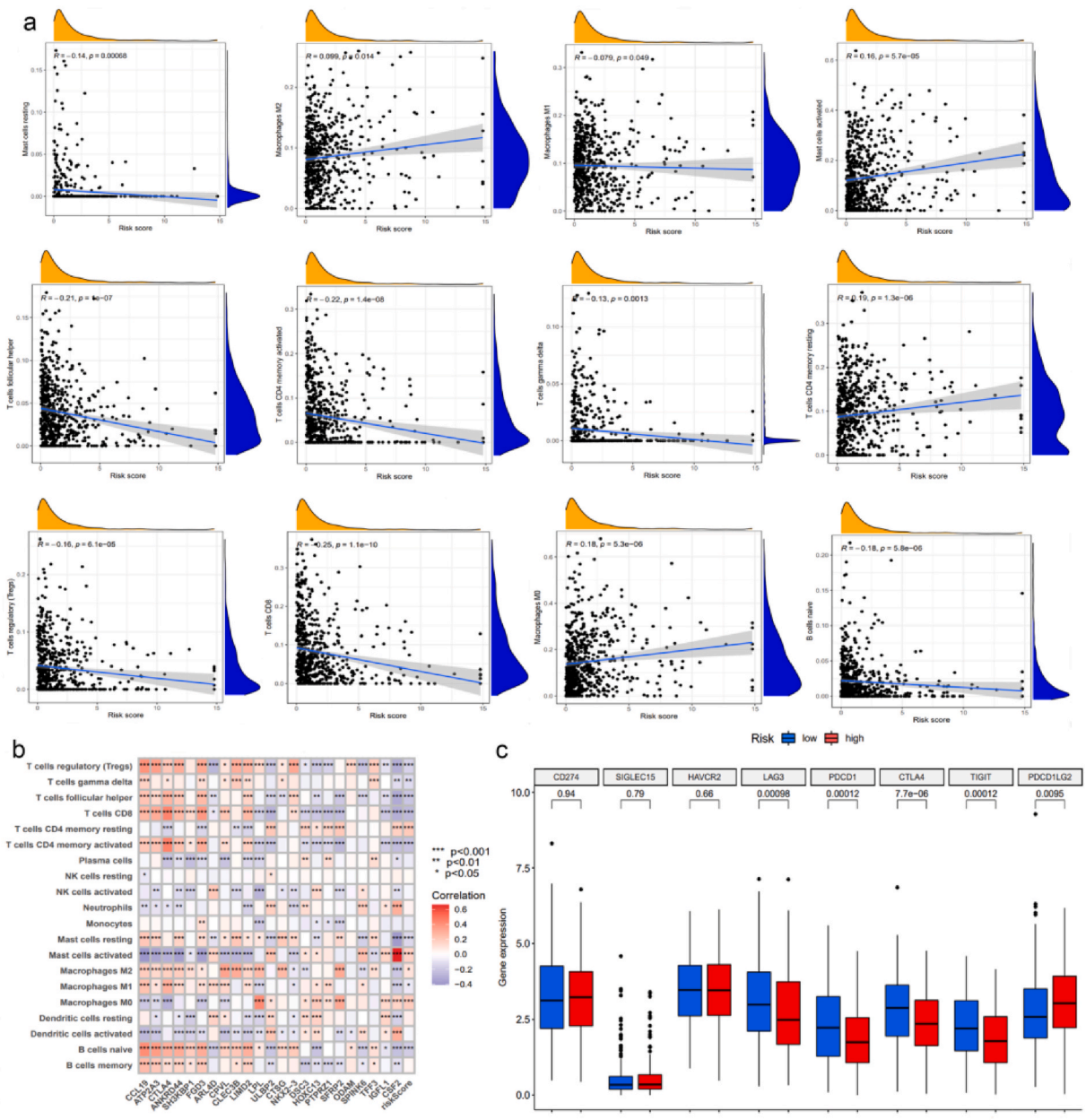

Fig. 8. Differences in TME and immune checkpoint between the two risk score groups. (a) Relationship between risk score and immune infiltrating cells. (b) Correlation between immune cell and risk genes. (c) Differences in immune checkpoint expression between two different risk score groups.

elimination of tumor cells [39]. In our study, subtype B in TRG typing and the low-risk score subtype were associated with immune activation features, whereas subtype A and high-risk score subtypes were associated with immunosuppressive features. $CD8^+$ T cells, which are capable of killing tumor cells, have been shown to serve as a prognostic indicator of tumors and their therapeutic response [40,41]. Patients with subtype B and low-risk scores with a better prognosis had a higher infiltration rate of activated CD8 + T cells, and subtype B patients had higher levels of immune checkpoints, suggesting that immunotherapy effects may also be better. B lymphocytes play a key role in patients with HNSC, and a high density of B lymphocytes predicts a good prognosis [42] and response to PD-1 blockade immunotherapy [43,44]. This study showed that the abundance of B cells in subtype B and low-risk groups with better survival rates was significantly higher than that in subtype A and high-risk groups. This indicated that B cell abundance partially reflected the better prognosis and immunotherapy effects of HNSC. M1 and M2 in macrophages, M1 inhibits and M2 promotes tumor progression in macrophages [45,46]. The polarization of M1 macrophages by gene editing can promote an anti-tumor immune response [47]. The results showed that the low-risk group had more M1 macrophages, a better prognosis, and higher levels of most immune checkpoints. Immunotherapy has become a powerful tool for cancer treatment [48]. Cancer immunotherapy strategies

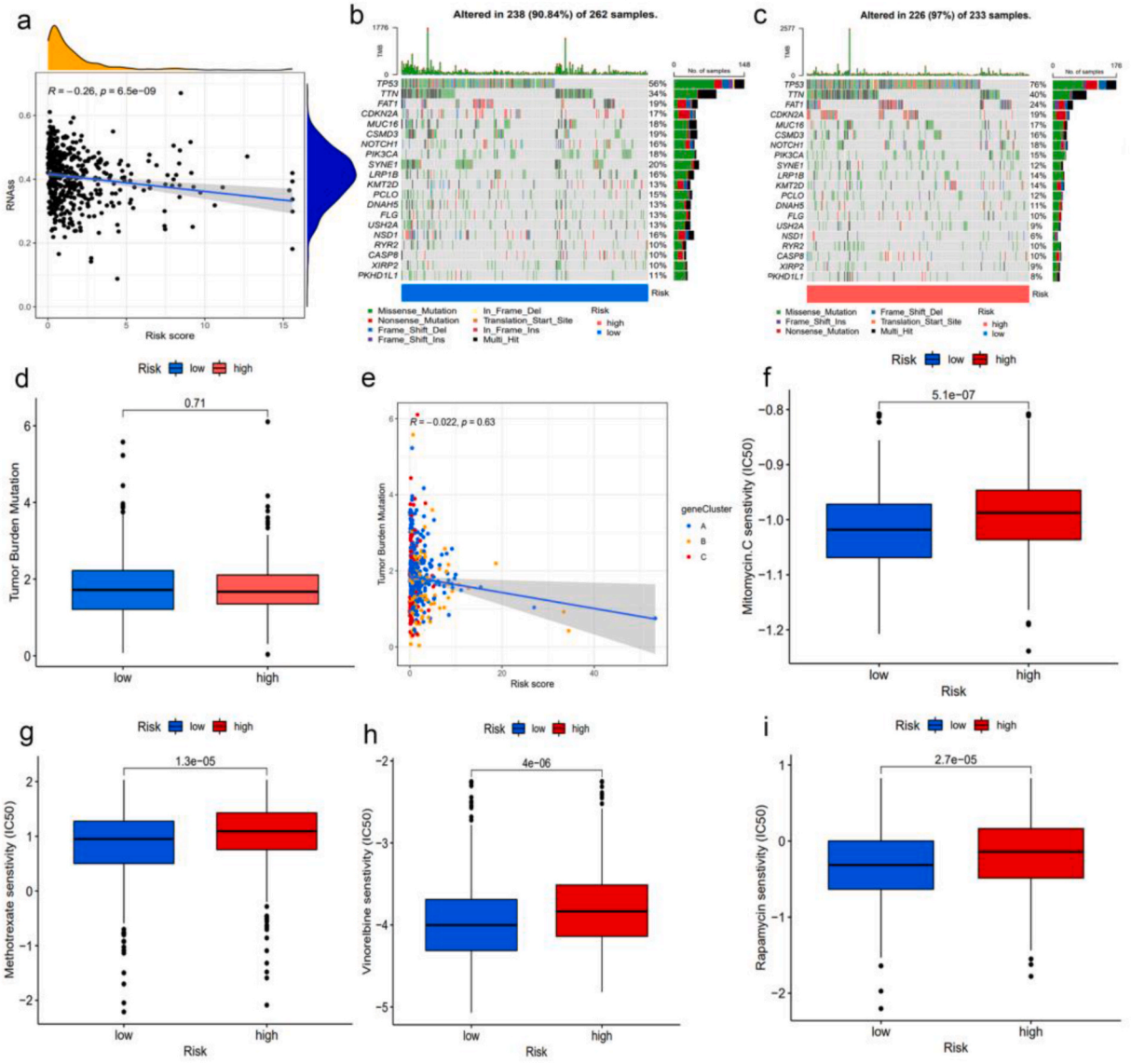

Fig. 9. Comprehensive analysis of the risk score in HNSC. (a) Correlation between risk score and CSC index. (b–c) The waterfall plot of somatic mutation features established with low- and high-risk group. Each column represented an individual patient. The upper barplot showed TMB, the number on the right indicated the mutation frequency in each gene. The right barplot showed the proportion of each variant type. (d) TMB in different risk score groups. (e) Spearman correlation analysis of the risk score and TMB. (f–i) Chemotherapy sensitivity in different risk score groups.

include ICIs, adoptive cell therapy, monoclonal antibodies, oncolytic virus immunotherapy, and vaccination [49]. ICIs are progressing rapidly, and have recently brought new light to the treatment of HNSC. In conclusion, low-risk patients are more likely to benefit from immunotherapy. Our study further revealed that T cells, B cells, and macrophages are involved in the anti-tumor process and may provide a new target for immunotherapy.

Cancer stem cells (CSCs) have self-renewal and tumorigenic properties, and their risk score is correlated with the CSC index. A comparison of the IC50 values between treatments showed that the low-risk group was more sensitive to these drugs. Therefore, CSC and IC50 may affect the development and treatment of HNSC. We then randomly assessed the expression levels of five prognostic markers of TRGs in HNSC. Moreover, 8 pairs of HNSC samples were collected in the First Affiliated Hospital of Anhui Medical University, and it was found that the expression levels of ULBP2, CLEC3B, CSF2, and FGD3 in HNSC cancerous tissues and adjacent tissues were significantly different. The results suggest that these four genes may be therapeutic targets for HNSC. ULBP2 has been found to be a prognostic marker for a variety of tumors [50,51], but whether it plays a role in HNSC remains unclear. *In vitro* experiments showed that the proliferation ability of ULBP2 knockdown HNSC cell lines was significantly reduced. These results suggest that these four genes, especially ULBP2, may play an important role in HNSC and may become a new therapeutic target for HNSC.

Our study had several limitations. First, our analysis was based on public databases, which may have led to an inherent selection

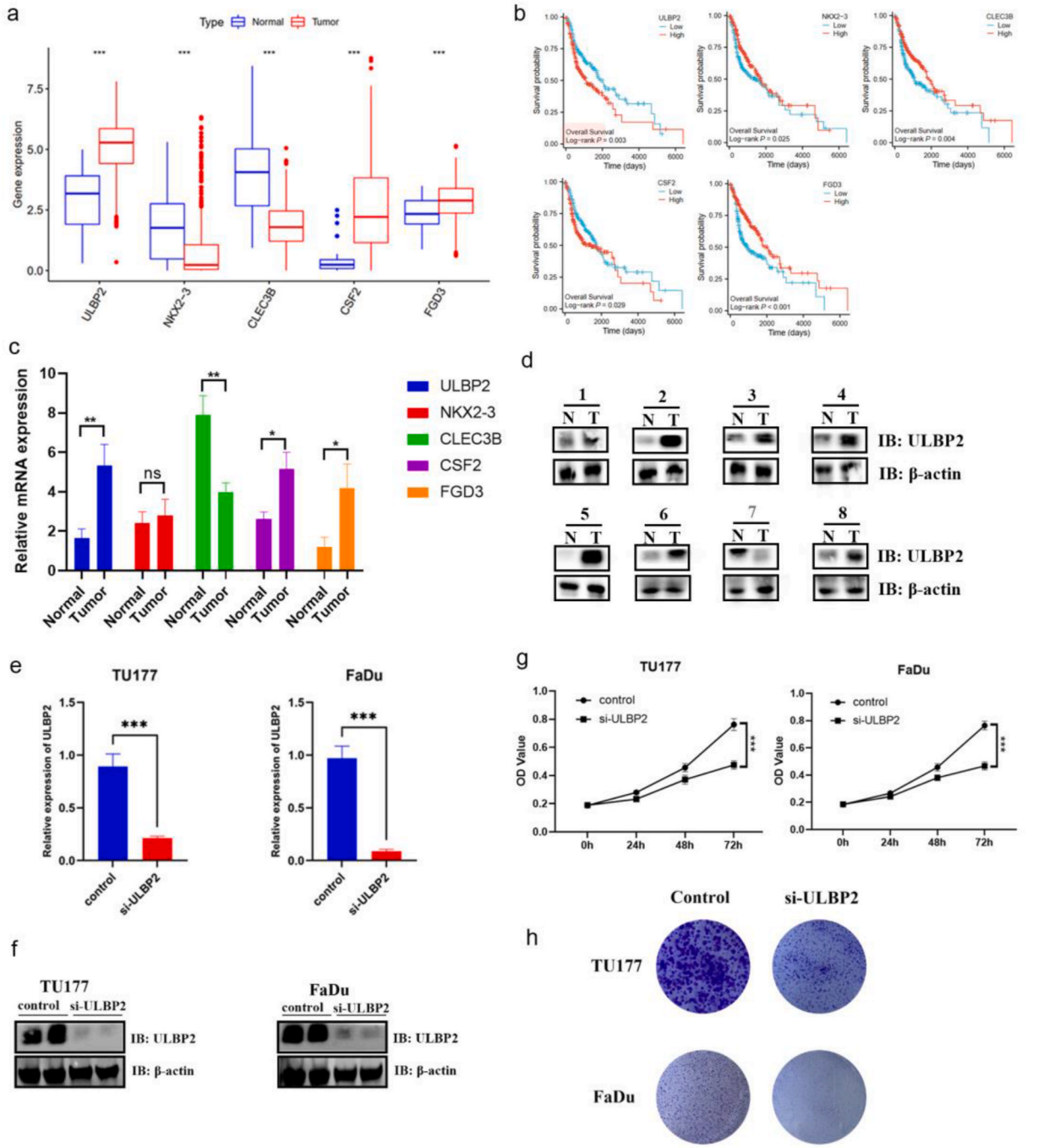

Fig. 10. Expression difference and function analysis of prognostic TRGs in tumor and normal cells. (a) Expression difference of some signature genes between normal and tumor tissues (TCGA). (b) The KM analysis evaluated the prognostic value of 5 TRGs (TCGA). (c) The relative RNA levels of ULBP2, NKX2-3, CLEC3B, CSF2 and FGD3 in tumor and adjacent normal tissues of HNSC patients were detected by q-PCR. (d) The protein expression of ULBP2 gene in 8 pairs of HNSC tumors and adjacent tissues was detected by Western blot. (e–f) The knockdown efficiency of si-ULBP2 was detected by q-PCR and Western blot in 2 HNSC cell lines. (g) MTT experiments showed that knocking down ULBP2 could inhibit cell viability. (h) Colony formation experiment showed that knocking down ULBP2 could decrease colony-forming abilities.

bias. Second, some key clinical features, such as surgery and chemotherapy, are not in the database, which may affect the accuracy of some clinical studies. Third, we need further studies to confirm this *in vitro* and in vivo.

5. Conclusions

In conclusion, our study on TRGs in patients with HNSC has shed light on the potential mechanisms affecting the TME, clinical features, and prognosis, and analyzed the potential usefulness of TRGs in immunotherapy. The results of this study reveal the important clinical prognostic role of TRGs and provide a foundation for further research and development of more effective treatment strategies for patients with HNSC.

Ethics approval and consent to participate

Studies involving human subjects were reviewed and approved by the Ethics Committee of the First Affiliated Hospital of Anhui Medical University, Ethics No. Quick-PJ 2023-07-60. Participants provided written informed consent to participate in the study.

Consent for publication

All authors agree to publish the paper.

Availability of data and materials

The datasets presented in this study can be found in online repositories. The names of the repository/repositories and accession number(s) can be found in the article.

Funding

This work was supported by the Provincial Natural Science Foundation of Anhui (No.2108085MH282).

CRediT authorship contribution statement

Wanjin Jiang: Writing – review & editing, Writing – original draft, Visualization, Validation. **Qi Yang:** Writing – review & editing, Writing – original draft, Visualization, Validation, Supervision, Software, Resources, Project administration, Methodology, Investigation, Funding acquisition, Data curation. **Xiaonan Yang:** Writing – original draft, Conceptualization. **Ruijia Gan:** Writing – original draft, Data curation. **Hongting Hua:** Writing – original draft, Visualization, Formal analysis. **Zhimin Ding:** Writing – original draft, Investigation, Formal analysis. **Dongyu Si:** Writing – original draft, Project administration, Methodology. **Xinbei Zhu:** Visualization, Investigation, Funding acquisition, Formal analysis. **Xu Wang:** Writing – review & editing, Writing – original draft, Visualization, Validation, Supervision. **Huabing Zhang:** Writing – review & editing, Writing – original draft, Visualization, Validation, Supervision. **Chaobing Gao:** Writing – review & editing, Writing – original draft, Visualization, Validation, Supervision, Funding acquisition.

Declaration of competing interest

The authors declare that they have no known competing financial interests or personal relationships that could have appeared to influence the work reported in this paper.

Acknowledgements

We acknowledged TCGA and GEO database for providing their platform and contributors for uploading their meaningful datasets. We would like to thank editage (www.editage.cn) for English language editing of this manuscript.

List of abbreviations

CNV	copy number variation
CSC	Cancer stem cell
DEG	differentially expressed gene
FDR	false discovery rate
GO	gene oncology
GSVA	gene set variation analysis
HNSC	head and neck squamous cell carcinoma
ICI	immune checkpoint inhibitor
KEGG	Kyoto Encyclopedia of Genes and Genomes
K-M	Kaplan-Meier

PCA principal component analysis
PD-1 programmed death-1
R/M HNSC recurrent/metastatic HNSC
ROC receiver operating characteristic
TME tumor microenvironment
TRG T-cell driver-related gene

Appendix A. Supplementary data

Supplementary data to this article can be found online at https://doi.org/10.1016/j.heliyon.2024.e34221.

References

[1] H. Sung, J. Ferlay, R.L. Siegel, M. Laversanne, I. Soerjomataram, A. Jemal, et al., Global cancer statistics 2020: GLOBOCAN estimates of incidence and mortality worldwide for 36 cancers in 185 countries, CA Cancer J Clin 71 (3) (2021) 209–249.
[2] D.E. Johnson, B. Burtness, C.R. Leemans, V.W.Y. Lui, J.E. Bauman, J.R. Grandis, Head and neck squamous cell carcinoma, Nat. Rev. Dis. Prim. 6 (1) (2020) 92.
[3] C.R. Leemans, P.J.F. Snijders, R.H. Brakenhoff, The molecular landscape of head and neck cancer, Nat. Rev. Cancer 18 (5) (2018) 269–282.
[4] J.D. Cramer, B. Burtness, Q.T. Le, R.L. Ferris, The changing therapeutic landscape of head and neck cancer, Nat. Rev. Clin. Oncol. 16 (11) (2019) 669–683.
[5] Z. Mei, J. Huang, B. Qiao, A.K. Lam, Immune checkpoint pathways in immunotherapy for head and neck squamous cell carcinoma, Int. J. Oral Sci. 12 (1) (2020) 16.
[6] B. Solomon, R.J. Young, D. Rischin, Head and neck squamous cell carcinoma: genomics and emerging biomarkers for immunomodulatory cancer treatments, Semin. Cancer Biol. 52 (Pt 2) (2018) 228–240.
[7] X. Lian, K. Yang, R. Li, M. Li, J. Zuo, B. Zheng, et al., Immunometabolic rewiring in tumorigenesis and anti-tumor immunotherapy, Mol. Cancer 21 (1) (2022) 27.
[8] G. Petroni, A. Buqué, L.M. Coussens, L. Galluzzi, Targeting oncogene and non-oncogene addiction to inflame the tumour microenvironment, Nat. Rev. Drug Discov. 21 (6) (2022) 440–462.
[9] B.A. Luca, C.B. Steen, M. Matusiak, A. Azizi, S. Varma, C. Zhu, et al., Atlas of clinically distinct cell states and ecosystems across human solid tumors, Cell 184 (21) (2021) 5482–5496.
[10] B.T. Grünwald, A. Devisme, G. Andrieux, F. Vyas, K. Aliar, C.W. McCloskey, et al., Spatially confined sub-tumor microenvironments in pancreatic cancer, Cell 184 (22) (2021) 5577–5592.
[11] K. Shah, A. Al-Haidari, J. Sun, J.U. Kazi, T cell receptor (TCR) signaling in health and disease, Signal Transduct Target Ther 6 (1) (2021) 412.
[12] A. Krug, A. Martinez-Turtos, E. Verhoeyen, Importance of T, NK, CAR T and CAR NK cell metabolic fitness for effective anti-cancer therapy: a continuous learning process allowing the optimization of T, NK and CAR-based anti-cancer therapies, Cancers 14 (1) (2021 Dec 30) 183.
[13] M. Legut, Z. Gajic, M. Guarino, Z. Daniloski, J.A. Rahman, X. Xue, et al., A genome-scale screen for synthetic drivers of T cell proliferation, Nature 603 (7902) (2022) 728–735.
[14] S.R. Li, Q.W. Man, B. Liu, Development and validation of a novel hypoxia-related signature for prognostic and immunogenic evaluation in head and neck squamous cell carcinoma, Front. Oncol. 12 (2022) 943945.
[15] J. Huang, Z. Xu, Z. Yuan, L. Cheng, C. Zhou, Y. Shen, Identification of cuproptosis-related subtypes and characterization of the tumor microenvironment landscape in head and neck squamous cell carcinoma, J. Clin. Lab. Anal. 36 (9) (2022) e24638.
[16] A. Koch, S.C. Joosten, Z. Feng, T.C. de Ruijter, M.X. Draht, V. Melotte, et al., Analysis of DNA methylation in cancer: location revisited, Nat. Rev. Clin. Oncol. 15 (7) (2018) 459–466.
[17] S.A. Lambert, A. Jolma, L.F. Campitelli, P.K. Das, Y. Yin, M. Albu, X. Chen, J. Taipale, T.R. Hughes, M.T. Weirauch, The human transcription factors, Cell 172 (4) (2018) 650–665.
[18] L.F. Spurr, R.R. Weichselbaum, S.P. Pitroda, Tumor aneuploidy predicts survival following immunotherapy across multiple cancers, Nat. Genet. 54 (12) (2022 Dec) 1782–1785.
[19] M.T. Fernandes, M.N. Ghezzo, A.B. Silveira, R.K. Kalathur, V. Póvoa, A.R. Ribeiro, et al., Lymphotoxin-β receptor in microenvironmental cells promotes the development of T-cell acute lymphoblastic leukaemia with cortical/mature immunophenotype, Br. J. Haematol. 171 (5) (2015) 736–751.
[20] L. Schneider, J. Liu, C. Zhang, A. Azoitei, S. Meessen, X. Zheng, et al., The role of interleukin-1-receptor-antagonist in bladder cancer cell migration and invasion, Int. J. Mol. Sci. 22 (11) (2021) 5875.
[21] H. Hayasaka, J. Yoshida, Y. Kuroda, A. Nishiguchi, M. Matsusaki, K. Kishimoto, et al., CXCL12 promotes CCR7 ligand-mediated breast cancer cell invasion and migration toward lymphatic vessels, Cancer Sci. 113 (4) (2022) 1338–1351.
[22] J. Wei, L. Long, W. Zheng, Y. Dhungana, S.A. Lim, C. Guy, et al., Targeting REGNASE-1 programs long-lived effector T cells for cancer therapy, Nature 576 (7787) (2019) 471–476.
[23] Y. Cai, Y. Hu, F. Yu, W. Tong, S. Wang, S. Sheng, et al., AHNAK suppresses ovarian cancer progression through the Wnt/β-catenin signaling pathway, Aging (Albany NY) 13 (20) (2021) 23579–23587.
[24] Q. Xu, J. Chen, S. Ni, C. Tan, M. Xu, L. Dong, et al., Pan-cancer transcriptome analysis reveals a gene expression signature for the identification of tumor tissue origin, Mod. Pathol. 29 (6) (2016) 546–556.
[25] A.M. Tsimberidou, E. Fountzilas, L. Bleris, R. Kurzrock, Transcriptomics and solid tumors: the next frontier in precision cancer medicine, Semin. Cancer Biol. 84 (2022) 50–59.
[26] C. Li, S. Chen, W. Jia, W. Li, D. Wei, S. Cao, et al., Identify metabolism-related genes IDO1, ALDH2, NCOA2, SLC7A5, SLC3A2, LDHB, and HPRT1 as potential prognostic markers and correlate with immune infiltrates in head and neck squamous cell carcinoma, Front. Immunol. 13 (2022) 955614.
[27] R. Ming, X. Li, E. Wang, J. Wei, B. Liu, P. Zhou, et al., The prognostic signature of head and neck squamous cell carcinoma constructed by immune-related RNA-binding proteins, Front. Oncol. 12 (2022) 795781.
[28] J. Chen, J. Yang, H. Li, Z. Yang, X. Zhang, X. Li, et al., Single-cell transcriptomics reveal the intratumoral landscape of infiltrated T-cell subpopulations in oral squamous cell carcinoma, Mol. Oncol. 15 (4) (2021) 866–886.
[29] C. Ma, H. Li, X. Li, S. Lu, J. He, The prognostic value of faciogenital dysplasias as biomarkers in head and neck squamous cell carcinoma, Biomark Med 13 (16) (2019) 1399–1415.
[30] H. Kasashima, A. Duran, A. Martinez-Ordoñez, Y. Nakanishi, H. Kinoshita, J.F. Linares, et al., Stromal SOX2 upregulation promotes tumorigenesis through the generation of a SFRP1/2-expressing cancer-associated fibroblast population, Dev. Cell 56 (1) (2021) 95–110.
[31] H. Li, R. Zhong, C. He, C. Tang, H. Cui, R. Li, et al., Colony-stimulating factor CSF2 mediates the phenotypic plasticity of small-cell lung cancer by regulating the p-STAT3/MYC pathway, Oncol. Rep. 48 (1) (2022) 122.
[32] Y. Jin, X. Qin, Integrated analysis of DNA methylation and mRNA expression profiles to identify key genes in head and neck squamous cell carcinoma, Biosci. Rep. 40 (1) (2020) BSR20193349.

[33] L.L. Fu, M. Yan, M.X. Ma, Y. Luo, M. Shao, M. Gosau, et al., DCBLD1 overexpression is associated with a poor prognosis in head and neck squamous cell carcinoma, Front. Immunol. 13 (2022) 939344.
[34] Z. Wang, S. Cheng, Y. Liu, R. Zhao, J. Zhang, X. Zhou, et al., Gene signature and prognostic value of ubiquitination-related genes in endometrial cancer, World J. Surg. Oncol. 21 (1) (2023) 3.
[35] M.D. Mody, J.W. Rocco, S.S. Yom, R.I. Haddad, N.F. Saba, Head and neck cancer, Lancet 398 (10318) (2021) 2289–2299.
[36] X. Zhang, M. Shi, T. Chen, B. Zhang, Characterization of the immune cell infiltration landscape in head and neck squamous cell carcinoma to aid immunotherapy, Mol. Ther. Nucleic Acids 22 (2020) 298–309.
[37] A.A. Bhat, P. Yousuf, N.A. Wani, A. Rizwan, S.S. Chauhan, M.A. Siddiqi, et al., Tumor microenvironment: an evil nexus promoting aggressive head and neck squamous cell carcinoma and avenue for targeted therapy, Signal Transduct Target Ther 6 (1) (2021) 12.
[38] A. Elmusrati, J. Wang, C.Y. Wang, Tumor microenvironment and immune evasion in head and neck squamous cell carcinoma, Int. J. Oral Sci. 13 (1) (2021) 24.
[39] K. Liu, J.J. Cui, Y. Zhan, Q.Y. Ouyang, Q.S. Lu, D.H. Yang, et al., Reprogramming the tumor microenvironment by genome editing for precision cancer therapy, Mol. Cancer 21 (1) (2022) 98.
[40] D. Hammerl, M.P.G. Massink, M. Smid, C.H.M. van Deurzen, H.E.J. Meijers-Heijboer, Q. Waisfisz, et al., Clonality, antigen recognition, and suppression of CD8+ T cells differentially affect prognosis of breast cancer subtypes, Clin. Cancer Res. 26 (2) (2020 Jan 15) 505–517.
[41] D.P. Hurkmans, M.E. Kuipers, J. Smit, R. van Marion, R.H.J. Mathijssen, P.E. Postmus, et al., Tumor mutational load, CD8+ T cells, expression of PD-L1 and HLA class I to guide immunotherapy decisions in NSCLC patients, Cancer Immunol. Immunother. 69 (5) (2020 May) 771–777.
[42] S. Zhang, B. Wang, F. Ma, F. Tong, B. Yan, T. Liu, et al., Characteristics of B lymphocyte infiltration in HPV+ head and neck squamous cell carcinoma, Cancer Sci. 112 (4) (2021) 1402–1416.
[43] S.S. Kim, S. Shen, S. Miyauchi, P.D. Sanders, I. Franiak-Pietryga, L. Mell, et al., B cells improve overall survival in HPV-associated squamous cell carcinomas and are activated by radiation and PD-1 blockade, Clin. Cancer Res. 26 (13) (2020) 3345–3359.
[44] A. Wieland, M.R. Patel, M.A. Cardenas, C.S. Eberhardt, W.H. Hudson, R.C. Obeng, et al., Defining HPV-specific B cell responses in patients with head and neck cancer, Nature 597 (7875) (2021) 274–278.
[45] S.M. Park, V.A. Do-Thi, J.O. Lee, H. Lee, Y.S. Kim, Interleukin-9 inhibits lung metastasis of melanoma through stimulating anti-tumor M1 macrophages, Mol. Cell. 43 (5) (2020) 479–490.
[46] N. Qiu, G. Wang, J. Wang, Q. Zhou, M. Guo, Y. Wang, et al., Tumor-associated macrophage and tumor-cell dually transfecting polyplexes for efficient interleukin-12 cancer gene therapy, Adv Mater 33 (2) (2021 Jan) e2006189.
[47] H. Yang, Q. Zhang, M. Xu, L. Wang, X. Chen, Y. Feng, et al., CCL2-CCR2 axis recruits tumor associated macrophages to induce immune evasion through PD-1 signaling in esophageal carcinogenesis, Mol. Cancer 19 (1) (2020) 41.
[48] R.S. Riley, C.H. June, R. Langer, M.J. Mitchell, Delivery technologies for cancer immunotherapy, Nat. Rev. Drug Discov. 18 (3) (2019) 175–196.
[49] L.B. Kennedy, A.K.S. Salama, A review of cancer immunotherapy toxicity, CA Cancer J Clin 70 (2) (2020) 86–104.
[50] M. Cadoux, S. Caruso, S. Pham, A. Gougelet, C. Pophillat, R. Riou, et al., Expression of NKG2D ligands is downregulated by β-catenin signalling and associates with HCC aggressiveness, J. Hepatol. 74 (6) (2021) 1386–1397.
[51] Z. Ye, H. Zhang, J. Liang, S. Yi, X. Zhan, Significance of logistic regression scoring model based on natural killer cell-mediated cytotoxic pathway in the diagnosis of colon cancer, Front. Immunol. 14 (2023) 1117908.